Electronic Supplementary Information

Steering CO$_2$ electroreduction selectivity towards CH$_4$ and C$_2$H$_4$ on tannic acid-modified Cu electrode

Keqiang Xu, [a] Jinhan Li, [a] Fangming Liu, [a] Wence Xu, [a] Tete Zhao, [a] Fangyi Cheng[* a,b]

[a]Key Laboratory of Advanced Energy Materials Chemistry (Ministry of Education), Renewable Energy Conversion and Storage Center, College of Chemistry, Nankai University, Tianjin 300071, China.

[b]Engineering Research Center of High-efficiency Energy Storage (Ministry of Education), Tianjin 300071, China.

E-mail: fycheng@nankai.edu.cn

Experimental section

Materials

$Cu(OAc)_2 \cdot H_2O$ (99.0%), $KHCO_3$ (99.0%), ethanol (99.5%), sodium ascorbate (SA, 98%), cetyltrimethylammonium chloride (CTAC, 96%), tannic acid (TA)were purchased from Alfa Aesar and used without purification.

Materials characterizations

Transmission electron microscopy (TEM) images were conducted on a FEI Talos F200X G2 with acceleration voltage 200 kV and scanning electron microscopy (SEM) images were achieved from JEOL JSM-7500F microscope with acceleration voltage 5 kV. X-ray diffraction (XRD) patterns were measured on a Rigaku Mini Flex 600 powder diffractometer with Cu Kα radiation. X-ray photoelectron spectroscopy (XPS) spectra were obtained on Perkin Elmer PHI 1600 ESCA system. Fourier transform infrared (FTIR) spectra were taken from Nicolet iS50, Thermo Fisher Scientific.

Sample preparation

Firstly, to prepare Cu nanoparticles (NPs), 0.72 g of CTAC, 154 mL of H_2O, and 2 mL of 0.1 M $Cu(OAc)_2 \cdot H_2O$ solution was mixed together and stirred for 15 min. Next, 4 mL of 0.5 M SA solution was added to above solution and continued to stir for 15 min. Then, the solution was heated to 100 °C and lasted for 180 min. After cooling to room temperature, Cu NPs were collected by centrifugation and washed by H_2O and ethanol at 8000 rpm for 6 min at least three times. Finally, Cu NPs were obtained after heating at 60 °C for 6 h under vacuum condition. Then, a desired amount of TA and Cu NPs

were mixed and ultrasonicated for 0.5 h in ethanol solution to prepare Cu-xTA (x represented the designed mass ratio of TA:Cu). Then the sample was centrifuged and dried at 60 °C for overnight under vacuum condition.

Electrode preparation

10 mg of nanoparticles was dispersed into 1 mL ethanol with 50 μL Nafion solution and sonicated for 1 h to obtain homogenous suspension. Then, 10 μL catalyst ink was dropped on glassy carbon electrode (6 mm in diameter) and dried at room temperature.

Electrochemical CO_2 reduction test in H-Cell

Electrochemical tests were performed in an H-type Cell separated by proton exchange membrane (Nafion-117) in CO_2-saturated 0.1 M $KHCO_3$ electrolyte with Parstat 4000 electrochemical workstation (AMETEK). Pt sheet and Ag/AgCl electrode (filled with saturated KCl solution) were used as counter electrode and reference electrode, respectively. Before CO_2RR test, the electrolyte was bubbled for at least 30 min with high-purity CO_2 (99.999%) to saturate electrolyte at a flow of 20 sccm with digital mass flow controller. In this work, all potentials were converted to reversible hydrogen electrode (RHE) unless mentioned by the following equation: $E_{RHE} = E_{Ag/AgCl} + 0.059pH + 0.197$.

Electrochemical CO_2 reduction test in flow cell

The 50 μL of catalyst ink was dropped onto the commercial Sigracet 29 BC carbon paper with a size of 15 x 15mm and dried at room temperature. Pt sheet and Ag/AgCl electrode (saturated KCl solution) were used as counter electrode and reference

electrode, respectively. The anode and cathode chamber was separated by anion exchange membrane (Fumapem FAA-3-PK-130), the membrane was pre-treated in 1 M KOH solution for 24 h at room temperature before usage. CO_2 gas was through the cathode side at a flow of 30 sccm during CO_2 electrolysis. The electrolyte both cathode and anode was 1 M $KHCO_3$ solution and circulated by peristaltic pump at a rate of 20 mL/min. The applied potentials were converted to RHE reference with iR_s compensation in following equation: $E_{RHE}=E_{Ag/AgCl}+0.059pH+0.197V-0.85iR_s$. The R_s was measured by electrochemical impedance spectroscopy operated from 100 KHz to 0.1 Hz with an amplitude of 10 mV at open-circuit voltage. Kinetic isotope effect (KIE) tests were performed by replacing H_2O with D_2O as solvent and other operations were identical.

Analysis of CO_2 reduction products

The gaseous products were quantified by on-line gas chromatography (GC 2014C) equipped with flame ionization detector (FID) for CO, CH_4, C_2H_4 and thermal conductivity detector (TCD) for H_2. Liquid products were determined by ^{1}H-NMR on Bruker AVANCE III 400MHz. The method was as follows: 600 μL electrolyte was mixed with 100 μL D_2O and 1mM of DMSO was used as internal standard, the procedure was set with water suppression for 64 scans. Faradaic efficiency (FE) of gaseous and liquid products were calculated as followed, respectively.

$$FE_{gas}=\frac{ZnF}{Q}=\frac{ZPV_0VF}{RTQ}$$

Z: transfer electron number for specific product,

n: mole for specific product,

F: Faraday constant,

P: 101325 Pa,

V_0: volume of gaseous product measured by GC,

V: volume of CO_2 through digital mass flow controller during CO_2RR,

R: gas constant (8.314 J/(mol·K)),

T: room temperature (298 K),

Q: quantity of charges during the CO_2 electrolysis.

$$FE_{liquid} = \frac{ZnF}{Q} = \frac{ZC_{DMSO}S_{product}H_{DMSO}VF}{S_{DMSO}H_{product}Q}$$

Z: transfer electron number for specific product,

n: mole for specific product,

F: Faraday constant,

C_{DMSO}: concentration of DMSO internal standard,

V: volume of electrolyte in the cathode chamber,

$S_{product}$ and S_{DMSO}: peak areas of product and DMSO in the ^{1}H-NMR spectrum, respectively,

$H_{product}$ and H_{DMSO}: numbers of hydrogen in the product and DMSO, respectively,

Q: quantity of charges during the CO_2 electrolysis.

The electrochemically active surface area (ECSA) tests

The electrochemically active surface area (ECSA) tests were performed using cyclic voltammetry (CV) with different scan rates in the range of 30-70 mV/s from 0.20 to 0.22 V.

OH$^-$ adsorption and desorption test

The OH⁻ adsorption measurements were carried out to explore the influence of OH⁻ behavior after TA-modified Cu NPs. Prior to test, electrolyte was bubbled for at least 30 min with Ar. The OH⁻ adsorption and desorption tests were measured using cyclic voltammetry (CV) from 0 to 0.8 V in Ar-saturated 0.1 M KOH solution.

In situ ATR-SEIRS spectroscopy

The Au film was deposited on Si prism using reported chemical reduction method. Before Au film deposition, the Si prism was soaked in aqua regia solution for 30 min and washed by deionized water. Then Si prism was polished with Al_2O_3 powder for 10 min and sonicated in acetone and deionized water for three times in sequence. Next, Si prism was treated by fresh piranha solution for 30 min and NH_4F solution (40 %) for 5 min. Finally, Si prism was immersed into 15 mL Au plating liquid solution (0.01mM) mixed with 3.4 mL 2% HF solution for 5 min and washed by deionized water.

In situ ATR-SEIRS spectra were performed by the Fourier Transform Infrared Spectrophotometer (FTIR, Nicolet iS50, Thermo Fisher Scientific) with mercury cadmium telluride (MCT) detector. All spectra were conducted in transmission units and spectral resolution was set to 4 cm^{-1} at an incidence angle of 60°. Before experiment, CO_2 gas was bubbled into in 0.1 M $KHCO_3$ at least 30 min to make electrolyte saturate and remove the residual air. CO_2 gas was continuously bubbled during the test. The spectra were measured by between -0.5 and -1.4 V and reference spectra was obtained at -0.1 V.

Computational section

The density functional theory (DFT) calculation was performed by the Vienna Ab

initio Simulation package (VASP). We optimized the adsorption configuration of TA on Cu and studied the *CO adsorption and *CO hydrogenation energy. The DFT calculation was adopted by the Perdew, Burke, Ernzerhof exchange-correlation potential and the energy cut-off of 450 eV was set to deal with the electron–ion interactions. A 4 layer (7 × 7) of Cu (111) supercell with the top two layers relaxed was built as the exposed Cu (111) surface model and the 15 Å was set along the z-direction. The Visualization for Electronic and Structural Analysis (VESTA) was used to visualize the optimized structure in the work.[1]
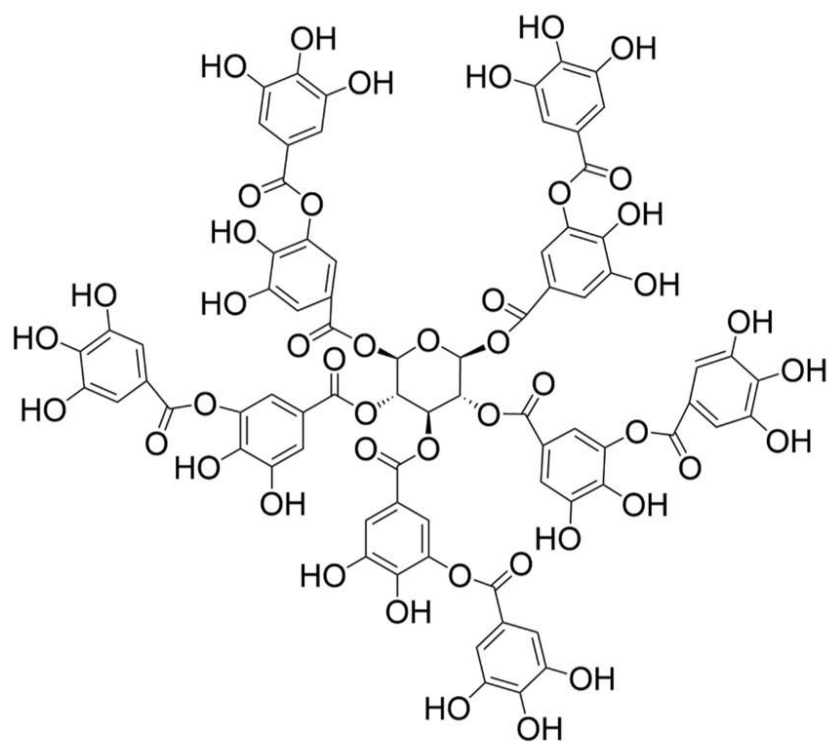
Figure S1 Molecular structure of TA molecule.
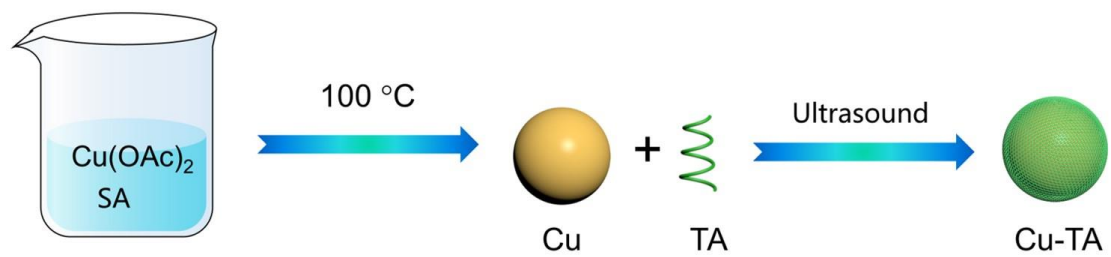
Figure S2 Synthesis process for Cu and Cu-TA NPs.
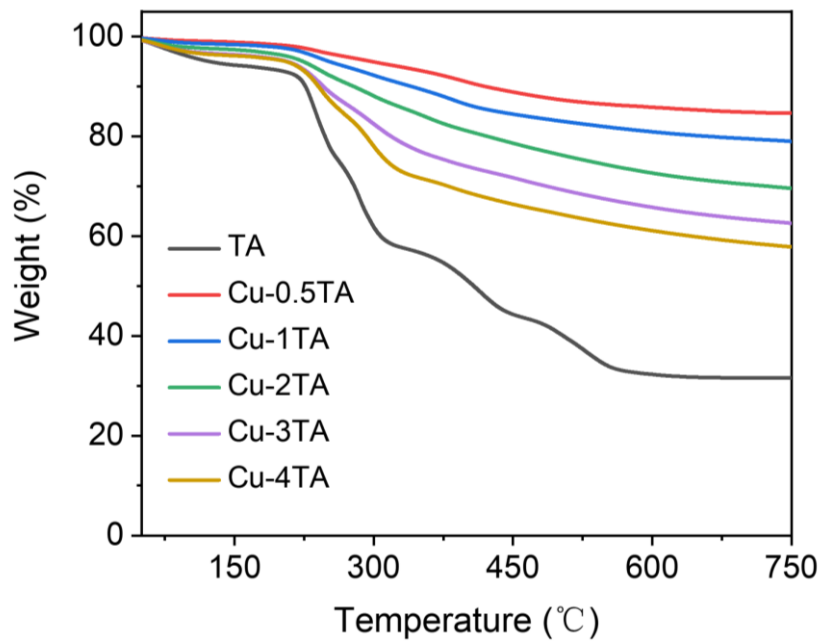
Figure S3 TGA curves of TA and Cu-xTA (x from 0.5 to 4) NPs under Ar condition.
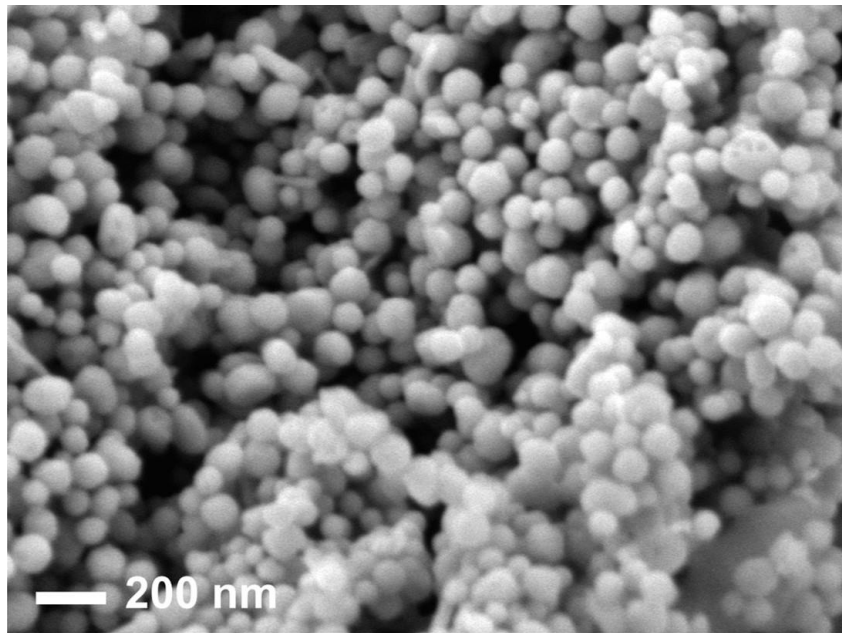
Figure S4 SEM image of prepared Cu NPs.
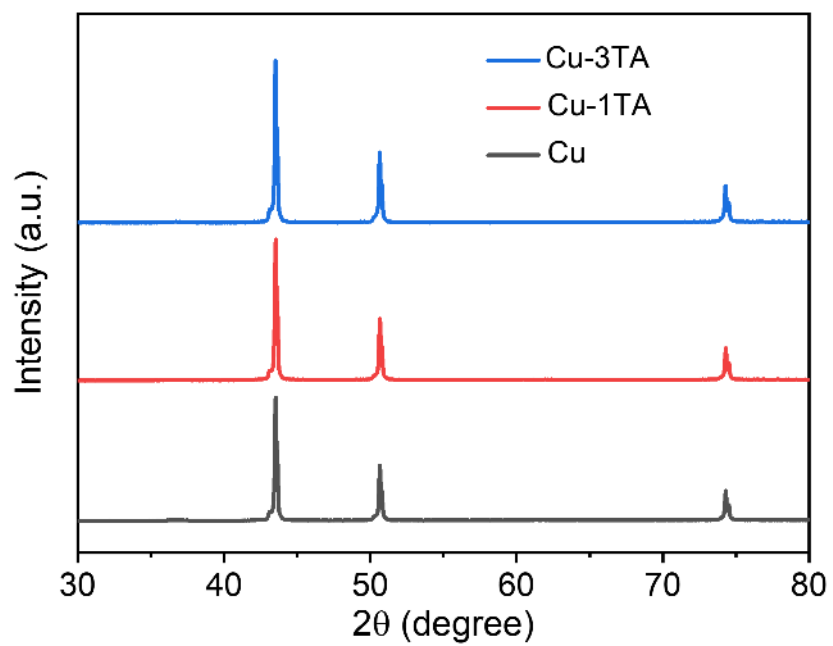
Figure S5 XRD pattern of Cu, Cu-1TA and Cu-3TA NPs.
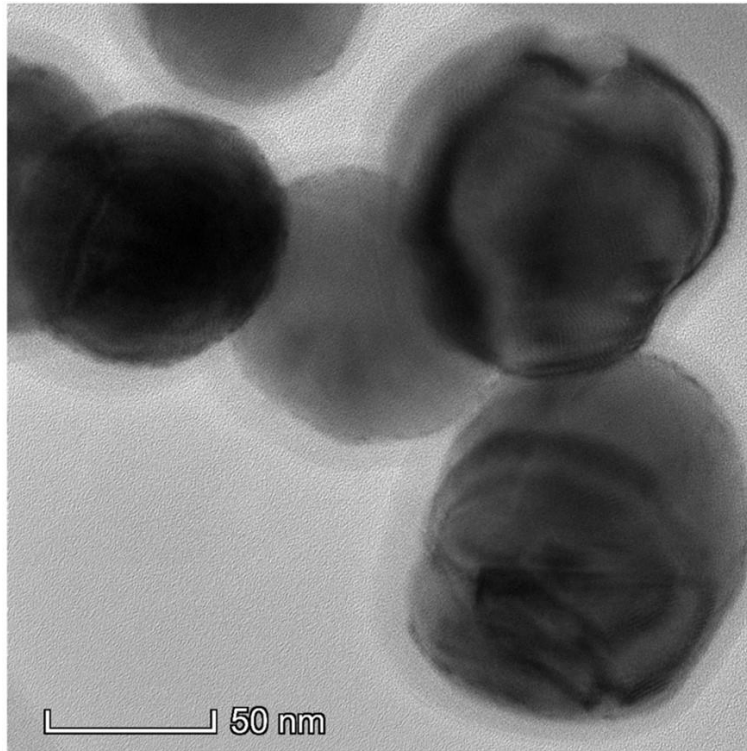
Figure S6 TEM image of prepared Cu-3TA NPs.
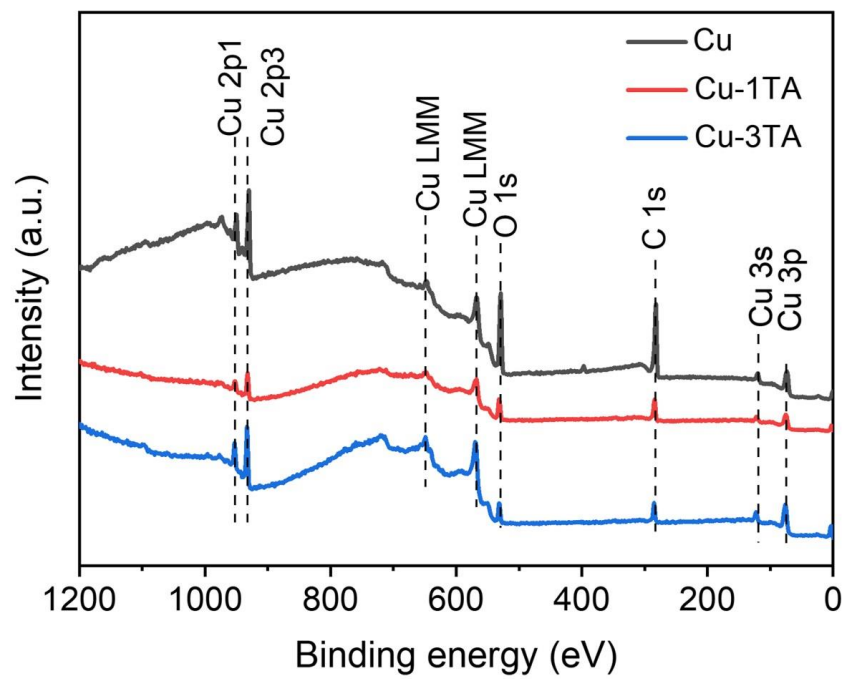
Figure S7 XPS survey of Cu, Cu-1TA and Cu-3TA NPs.
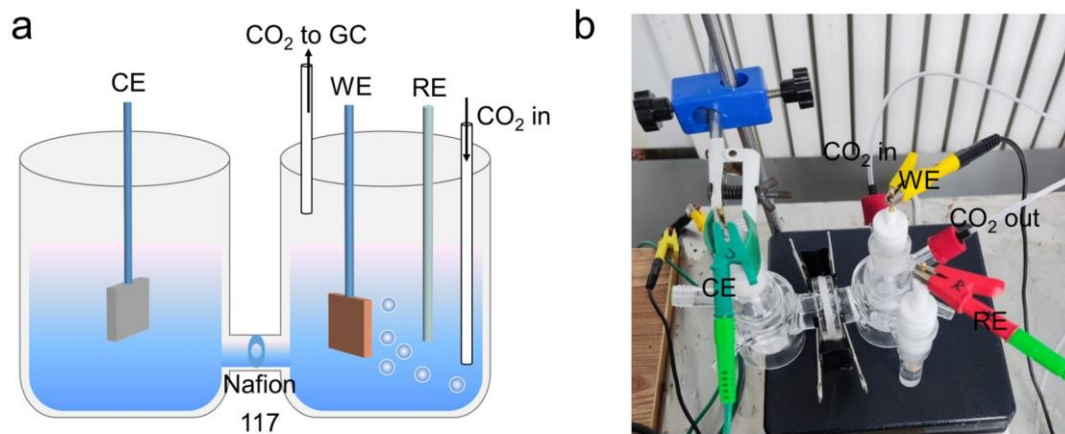
Figure S8 (a, b) Schematic diagram of H-Cell and corresponding photo in our experiment.
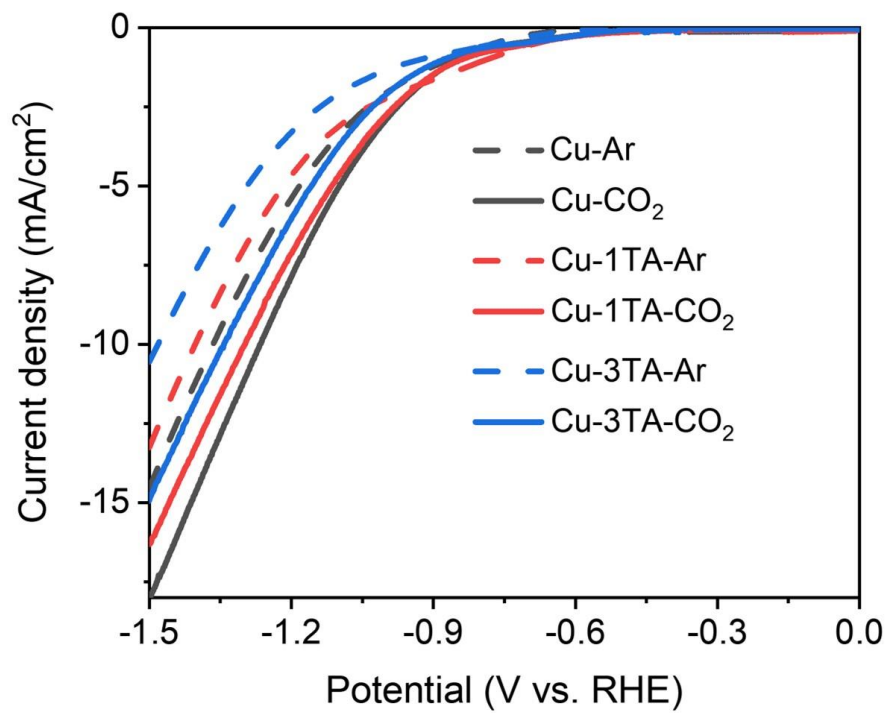
Figure S9 LSV curves of catalysts in Ar or CO_2-saturated 0.1 M $KHCO_3$ solution.
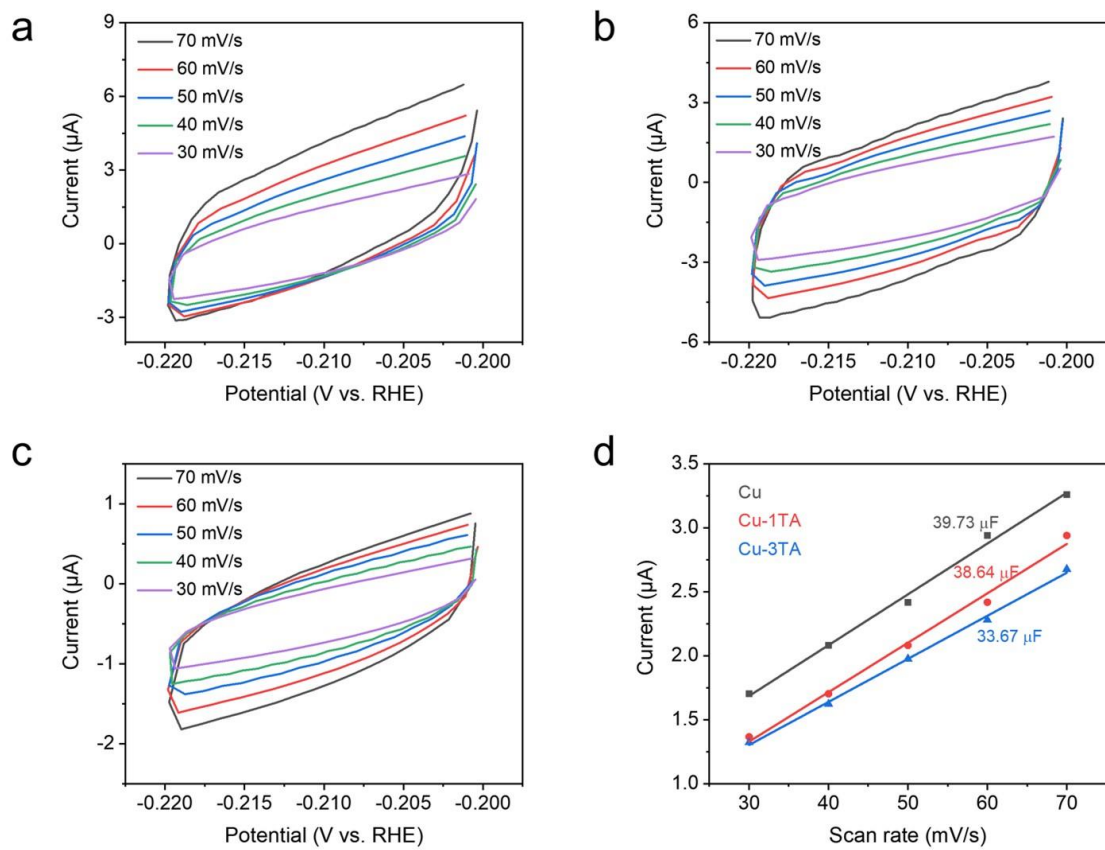
Figure S10 CV curves with different scan rates for (a) Cu, (b) Cu-1TA and (c) Cu-3TA catalysts. (d) The corresponding fitting current versus scan rates.

a
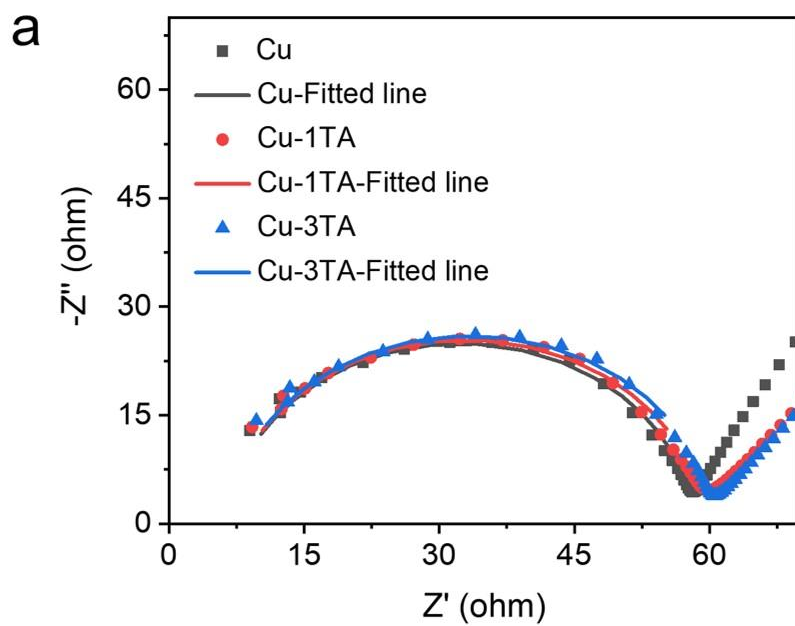
b

	Cu	Cu-1TA	Cu-3TA
R_s	6.55	6.39	6.53
R_{ct}	51.57	52.92	53.69

Figure S11 (a) Nyquist plots of catalysts determined at open circuit voltage. (b) The corresponding fitted values in H-Cell.
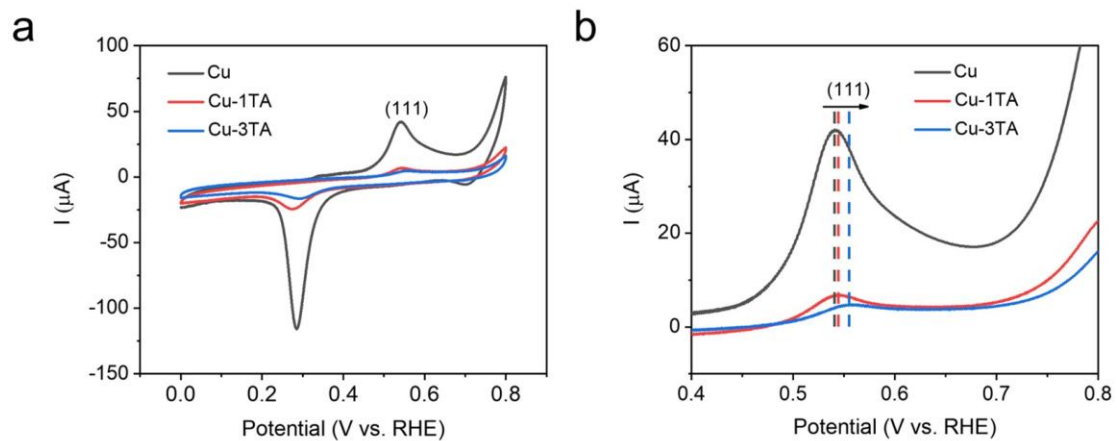
Figure S12 (a, b) CV and LSV curves of catalysts in Ar-saturated 0.1 M KOH solution at the scan rate of 50 mV/s.
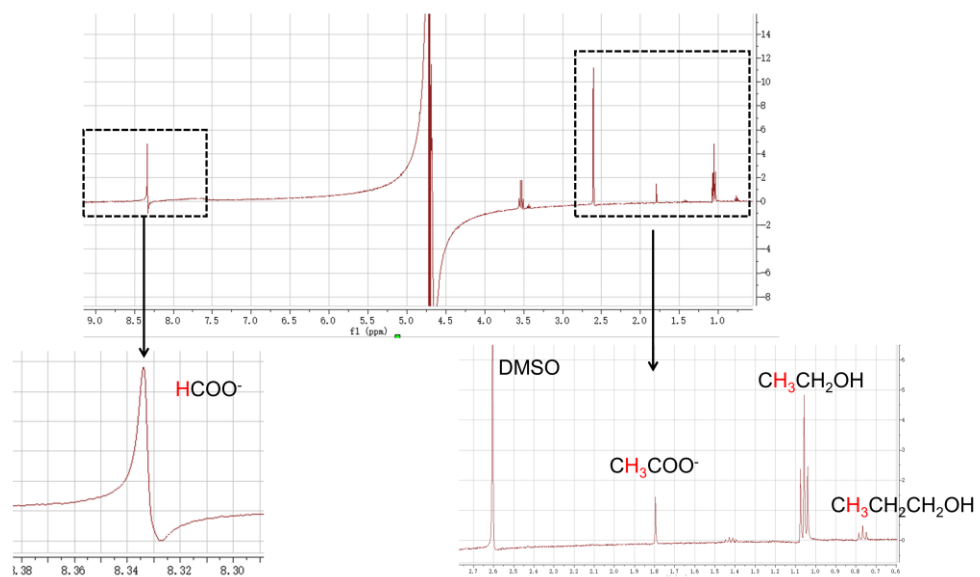
Figure S13 ^{1}H-NMR spectra of liquid products after electrolysis for Cu catalyst at -0.85 V in flow cell.
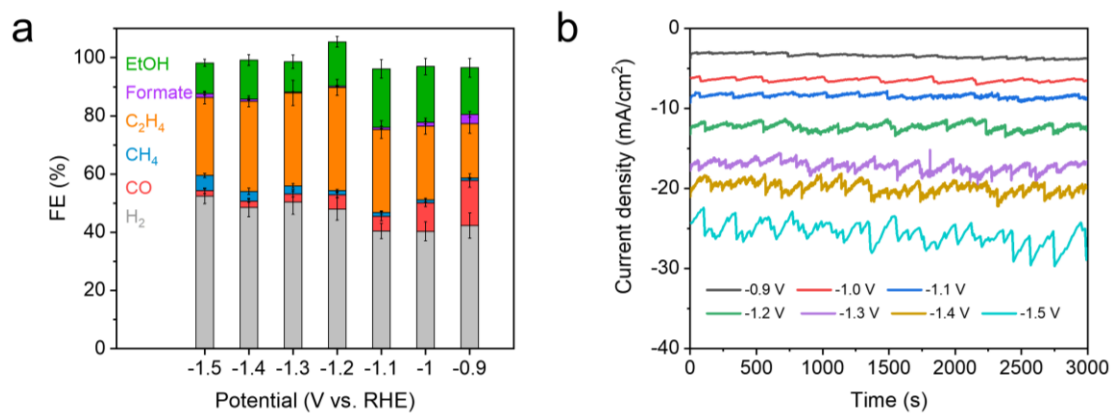
Figure S14 (a) FE of products on Cu catalyst under different applied potential and (b) corresponding chronoamperometry curves in CO_2-saturated 0.1 M $KHCO_3$ solution in H-Cell.
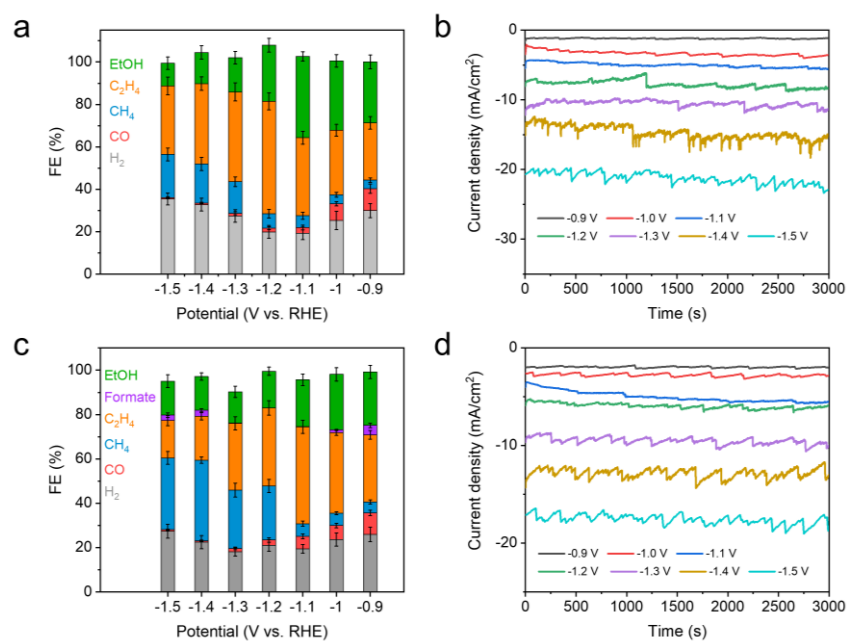
Figure S15 FE of products on (a) Cu-1TA and (c) Cu-3TA catalyst at different applied potential and (b, d) corresponding chronoamperometry curves in CO_2-saturated 0.1 M $KHCO_3$ solution in H-Cell.
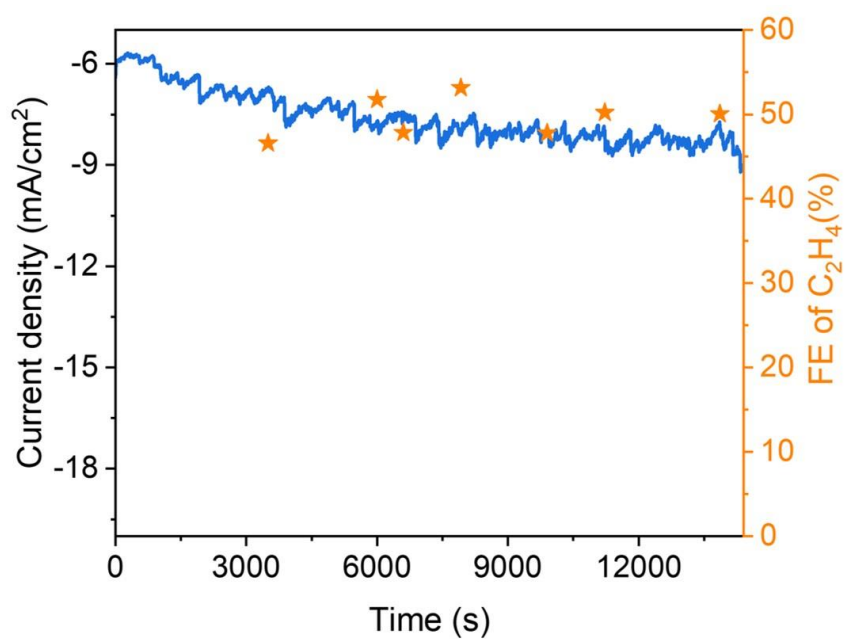
Figure S16 Chronoamperometry curve and FE of C$_2$H$_4$ for Cu-1TA catalyst at -1.2 V for

14400 s in H-Cell.
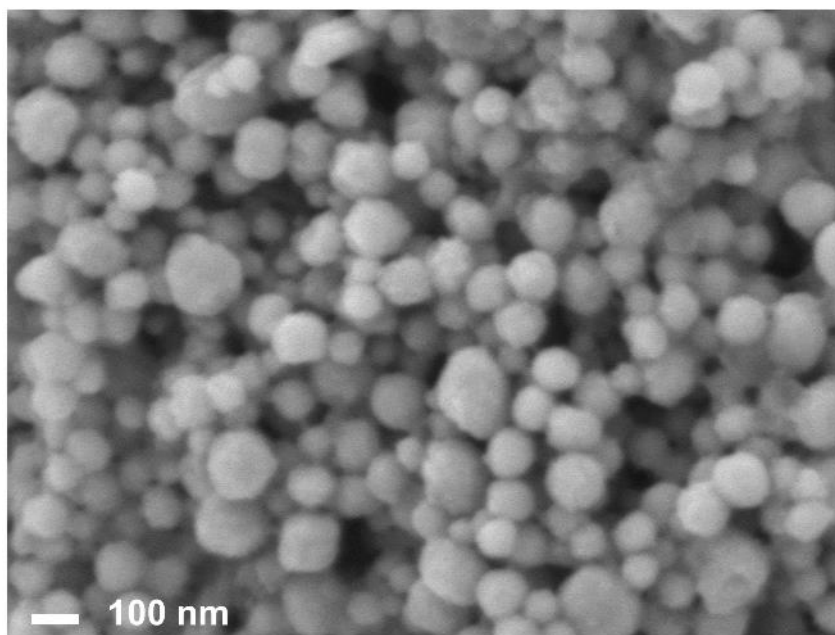
Figure S17 SEM image of Cu-1TA catalyst after stability test.
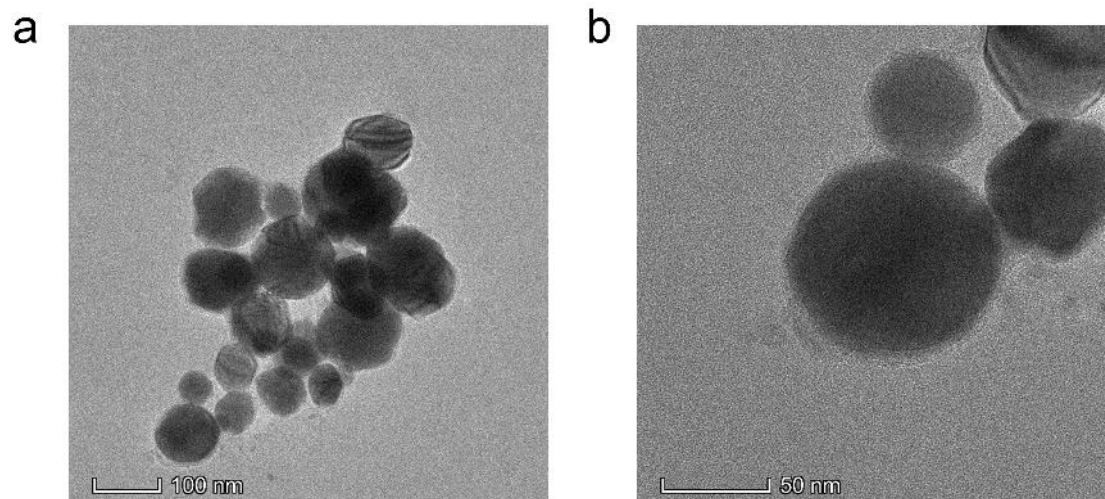
Figure S18 (a, b) TEM images of Cu-1TA catalyst after stability test.
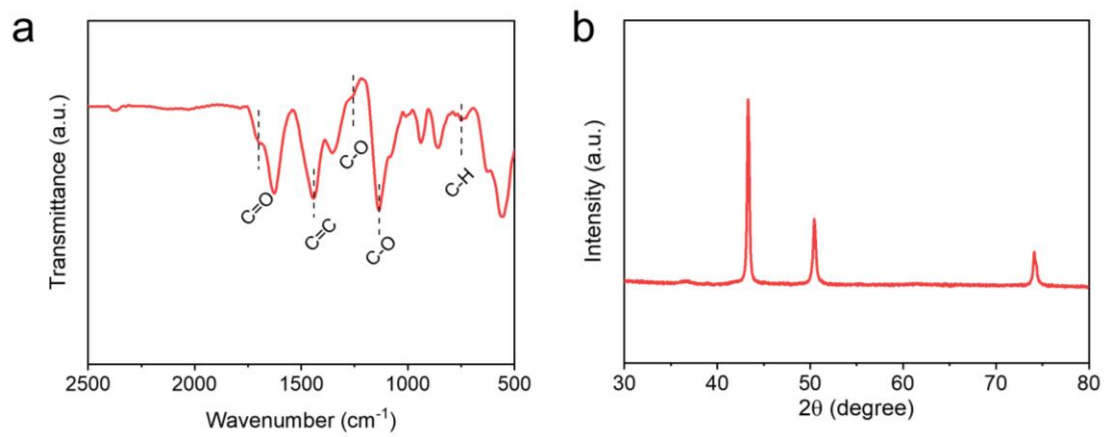
Figure S19 (a, b) FTIR and XRD curves of Cu-1TA catalyst after stability test.

Figure S20 (a, b) Scheme of flow cell reactor and corresponding photo in our work.
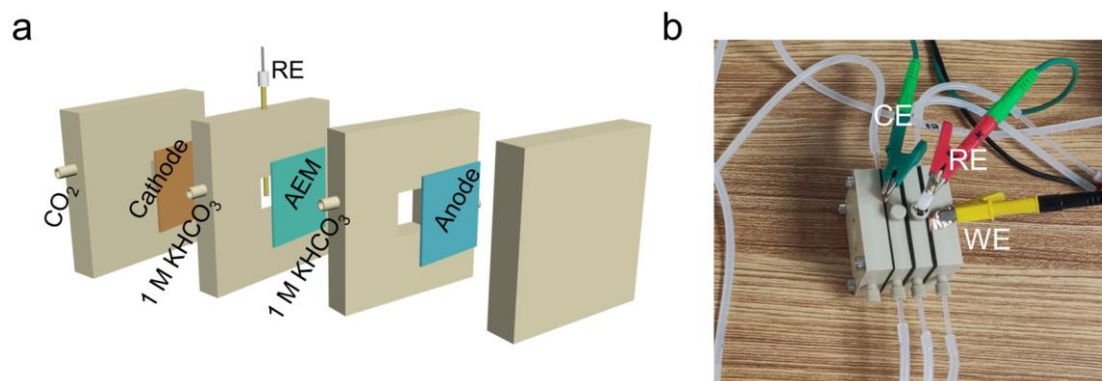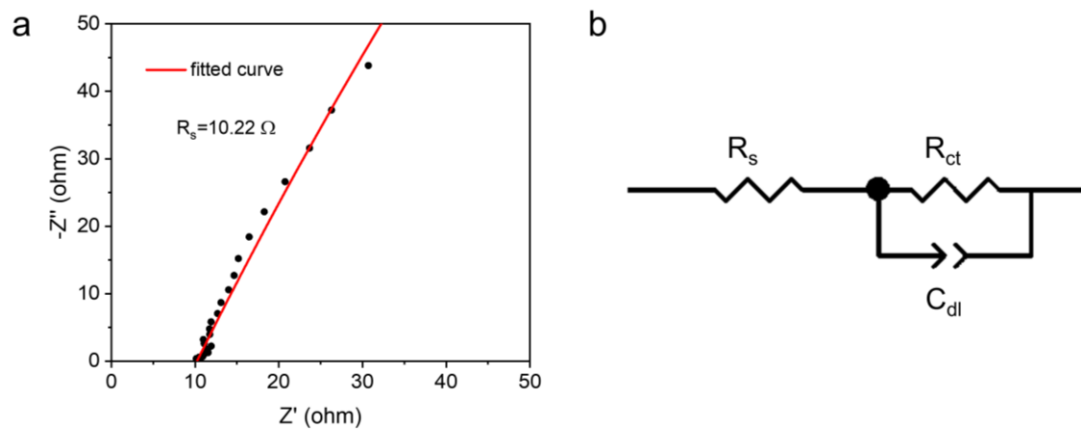
Figure S21 (a) Nyquist plots of catalysts determined at open circuit voltage and (b) the corresponding equivalent circuit diagram in flow cell reactor.
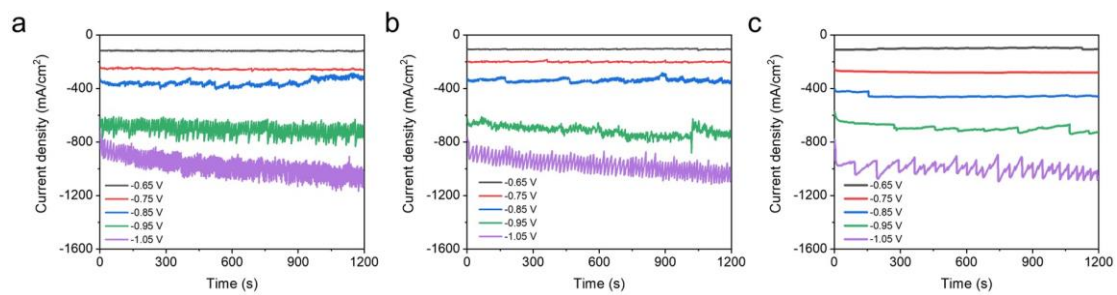
Figure S22 Chronoamperometry curves of (a) Cu, (b) Cu-1TA and (c) Cu-3TA catalyst under different potentials in flow cell.
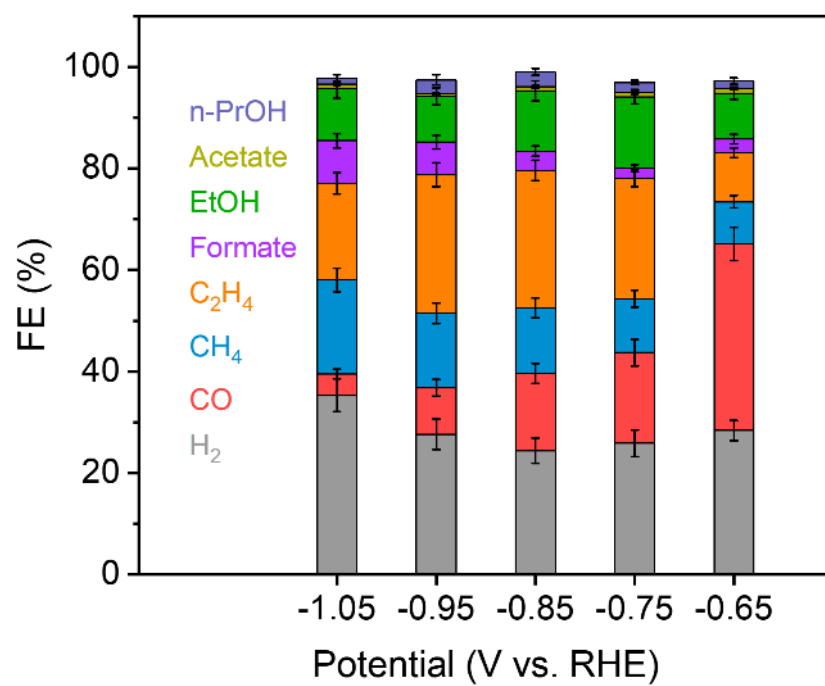
Figure S23 FE of products on Cu catalyst at different applied potential in flow cell.
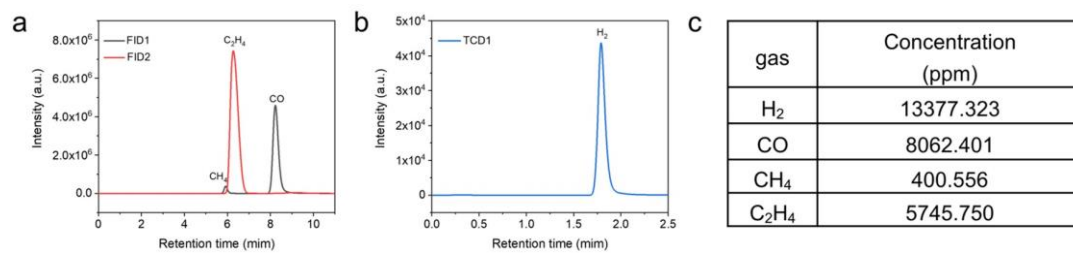
Figure S24 (a, b) Representative GC profiles of gaseous products on Cu-1TA catalyst at

-0.85 V and (c) corresponding concentration in flow cell.
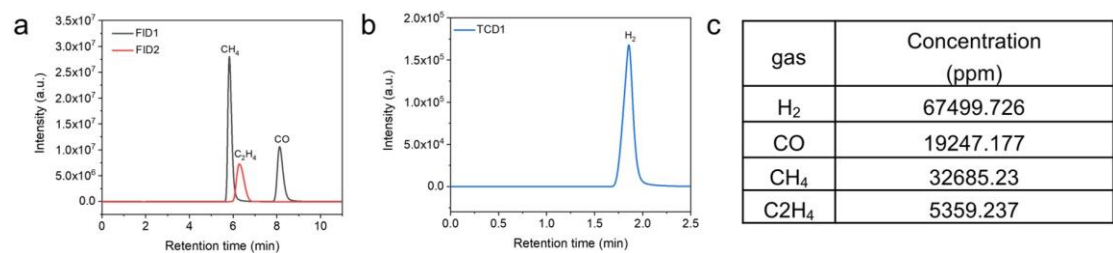
Figure S25 (a, b) Representative GC profiles of gaseous products on Cu-3TA catalyst at

-1.05 V and (c) corresponding concentration in flow cell.
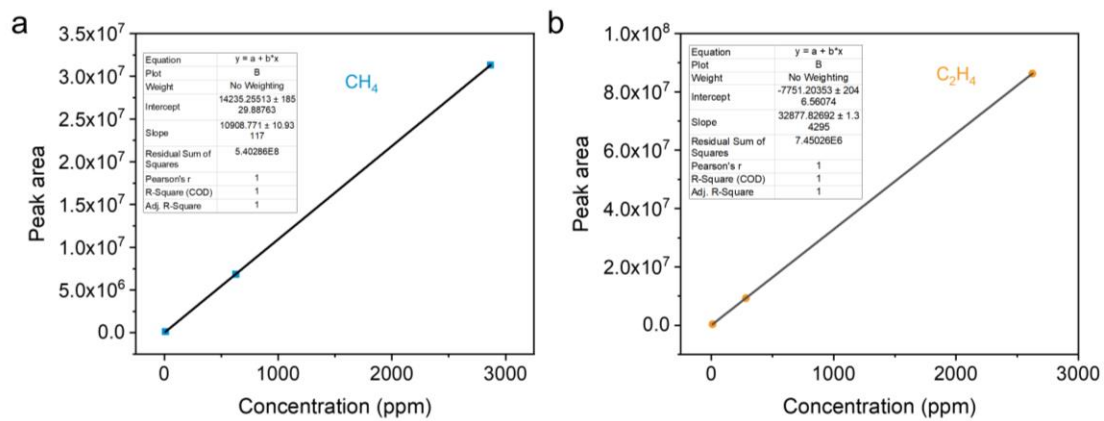
Figure S26 Standard curves of (a) CH_4 and (b) C_2H_4 components for GC analysis.
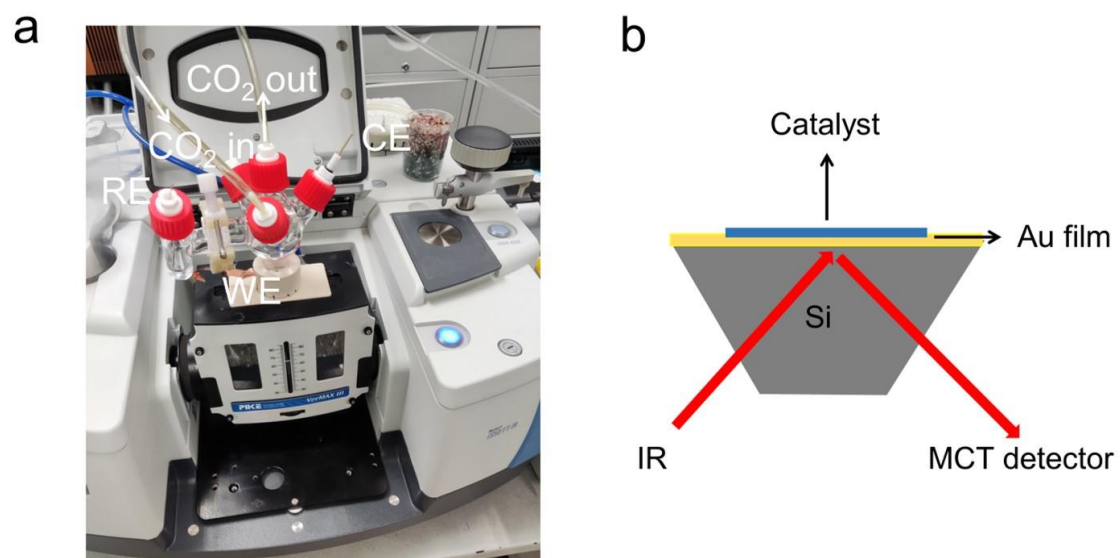
Figure S27 (a, b) Photo of the in situ ATR-SEIRAS setup and corresponding working mechanism.
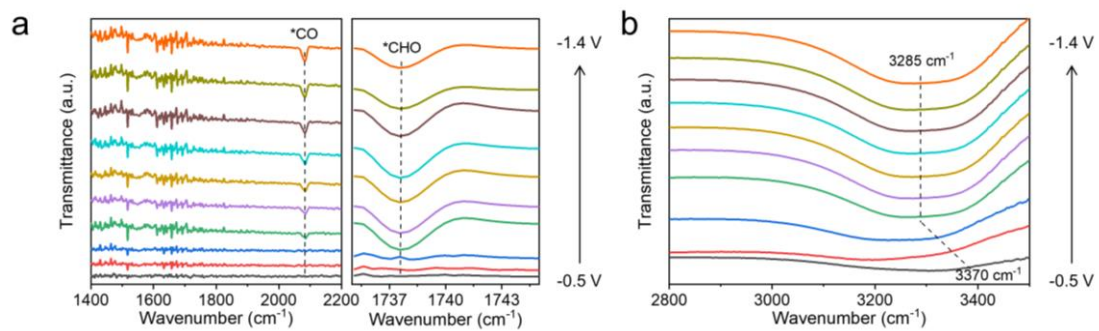
Figure S28 In situ ATR-SEIRS spectra of Cu-1TA catalyst in CO$_2$-saturated 0.1 M KHCO$_3$

solution.
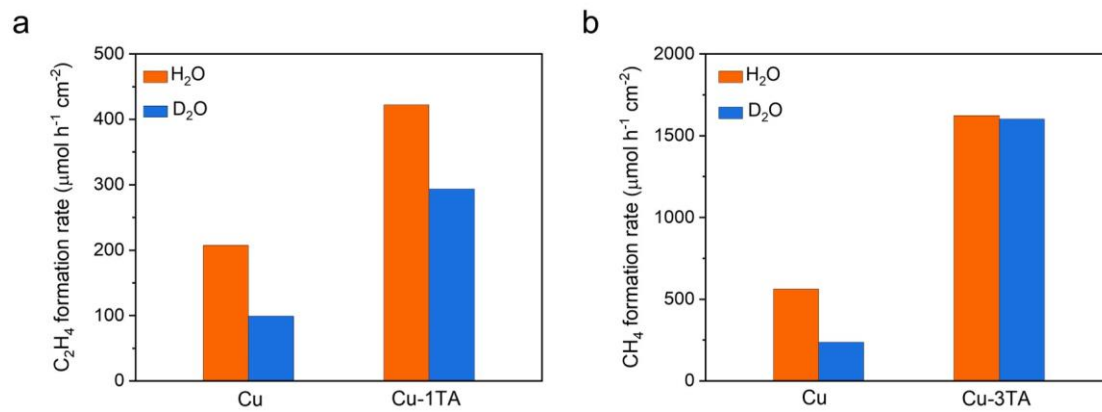
Figure S29 (a) Formation rate of C_2H_4 in H_2O and D_2O as solvent for Cu and Cu-1TA catalysts at -0.85 V and (b) formation rate of CH_4 in H_2O and D_2O as solvent for Cu and Cu-3TA catalysts at -1.05 V.
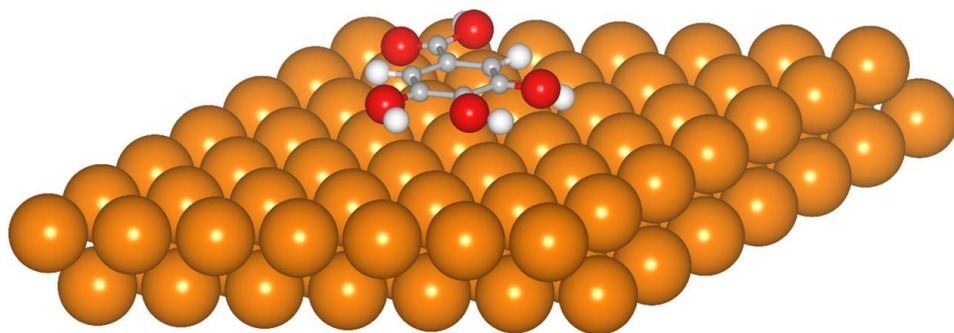
Figure S30 Optimized adsorption configuration of TA on Cu (111) facet.
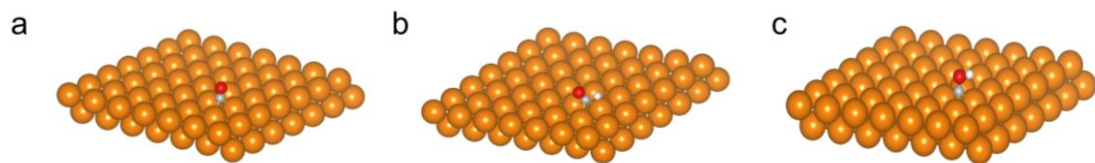
Figure S31 Optimized adsorption configuration of (a) *CO, (b) *CHO and (c) *COH intermediate on Cu (111) facet.
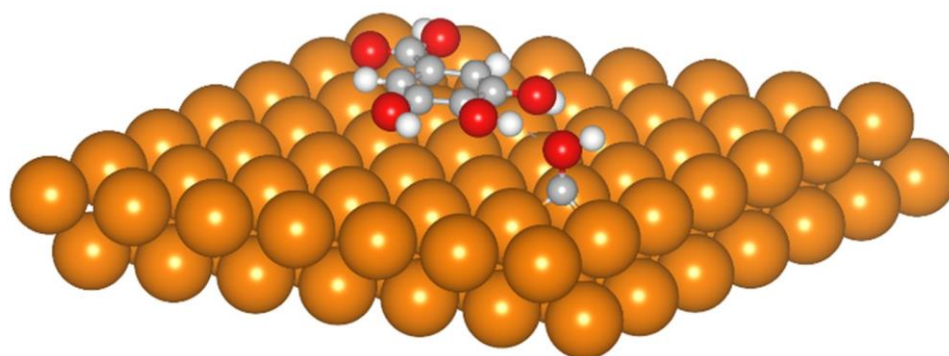
Figure S32 Optimized adsorption configuration of *COH intermediate on Cu-TA catalyst.

Table 1 Performance comparison of CO_2RR to C_2H_4 on molecule modified Cu-based catalysts.

Catalyst	FE (%)	Electrolyzer	Electrolyte	Ref.
Cu-1TA	53	H-Cell	0.1 M $KHCO_3$	This work
EDTA-Modified Cu	50.1	H-Cell	0.1 M $KHCO_3$	2
Cu-PANI	48.8	H-Cell	0.1 M $KHCO_3$	3
Cu-N-arylpyridinium	72	flow cell	1M $KHCO_3$	4
Cu-polyamine	87	flow cell	10 M KOH	5
Cu-copolymer	55	H-Cell	0.1 M $KHCO_3$	6
aromatic doped Cu-Ag	51	MEA Cell	0.1 M $KHCO_3$	7
ionic liquid on Cu	77.3	H-Cell	0.1 M $KHCO_3$	8

Table 2 Performance comparison of CO_2RR to CH_4 in flow cell.

Catalyst	FE (%)	j (mA/cm^2)	Electrolyte	Ref.
Cu-3TA	53.27	532.7	1 M KHCO$_3$	This work
Cu	48	108	1 M KHCO$_3$	9
CoO-Cu	60	135	1 M KHCO$_3$	10
Au in Cu	56	112	1M KHCO$_3$	11
Cu	48	120	1.5 M KHCO$_3$	12
Ag@Cu$_2$O	74	178	1 M KOH	13
Fe single atom on Cu	64	128	1 M KHCO$_3$	14
Amine-GQDs	63	170	1 M KOH	15

References

1. K. Momma and F. Izumi, VESTA 3 for three-dimensional visualization of crystal, volumetric and morphology data, *J. Appl. Crystallogr.*, 2011, **44**, 1272-1276.

2. J. Liu, J. Fu, Y. Zhou, W. Zhu, L.-P. Jiang and Y. Lin, Controlled Synthesis of EDTA-Modified Porous Hollow Copper Microspheres for High-Efficiency Conversion of CO_2 to Multicarbon Products, *Nano Lett.*, 2020, **20**, 4823-4828.

3. X. Wei, Z. Yin, K. Lyu, Z. Li, J. Gong, G. Wang, L. Xiao, J. Lu and L. Zhuang, Highly Selective Reduction of CO_2 to C_{2+} Hydrocarbons at Copper/Polyaniline Interfaces, *ACS Catal.*, 2020, **10**, 4103-4111.

4. F. Li, A. Thevenon, A. Rosas-Hernández, Z. Wang, Y. Li, C. M. Gabardo, A. Ozden, C. T. Dinh, J. Li, Y. Wang, J. P. Edwards, Y. Xu, C. McCallum, L. Tao, Z.-Q. Liang, M. Luo, X. Wang, H. Li, C. P. O'Brien, C.-S. Tan, D.-H. Nam, R. Quintero-Bermudez, T.-T. Zhuang, Y. C. Li, Z. Han, R. D. Britt, D. Sinton, T. Agapie, J. C. Peters and E. H. Sargent, Molecular tuning of CO_2-to-ethylene conversion, *Nature*, 2020, **577**, 509-513.

5. X. Chen, J. Chen, N. M. Alghoraibi, D. A. Henckel, R. Zhang, U. O. Nwabara, K. E. Madsen, P. J. A. Kenis, S. C. Zimmerman and A. A. Gewirth, Electrochemical CO_2-to-ethylene conversion on polyamine-incorporated Cu electrodes, *Nat. Catal.,* 2021, **4**, 20-27.

6. J. Wang, T. Cheng, A. Q. Fenwick, T. N. Baroud, A. Rosas-Hernández, J. H. Ko, Q. Gan, W. A. Goddard Iii and R. H. Grubbs, Selective CO_2 Electrochemical Reduction Enabled by a Tricomponent Copolymer Modifier on a Copper Surface, *J. Am. Chem. Soc.*, 2021, **143**, 2857-2865.

7. H. Wu, J. Li, K. Qi, Y. Zhang, E. Petit, W. Wang, V. Flaud, N. Onofrio, B. Rebiere, L. Huang, C.

Salameh, L. Lajaunie, P. Miele and D. Voiry, Improved electrochemical conversion of CO_2 to multicarbon products by using molecular doping, *Nat. Commun.,* 2021, **12**, 7210.

8. Y. Sha, J. Zhang, X. Cheng, M. Xu, Z. Su, Y. Wang, J. Hu, B. Han and L. Zheng, Anchoring Ionic Liquid in Copper Electrocatalyst for Improving CO_2 Conversion to Ethylene, *Angew. Chem. Int. Ed.*, 2022, **61**, e202200039.

9. X. Wang, A. Xu, F. Li, S.-F. Hung, D.-H. Nam, C. M. Gabardo, Z. Wang, Y. Xu, A. Ozden, A. S. Rasouli, A. H. Ip, D. Sinton and E. H. Sargent, Efficient Methane Electrosynthesis Enabled by Tuning Local CO_2 Availability, *J. Am. Chem. Soc.*, 2020, **142**, 3525-3531.

10. Y. Li, A. Xu, Y. Lum, X. Wang, S.-F. Hung, B. Chen, Z. Wang, Y. Xu, F. Li, J. Abed, J. E. Huang, A. S. Rasouli, J. Wicks, L. K. Sagar, T. Peng, A. H. Ip, D. Sinton, H. Jiang, C. Li and E. H. Sargent, Promoting CO_2 methanation via ligand-stabilized metal oxide clusters as hydrogen-donating motifs, *Nat. Commun.,* 2020, **11**, 6190.

11. X. Wang, P. Ou, J. Wicks, Y. Xie, Y. Wang, J. Li, J. Tam, D. Ren, J. Y. Howe, Z. Wang, A. Ozden, Y. Z. Finfrock, Y. Xu, Y. Li, A. S. Rasouli, K. Bertens, A. H. Ip, M. Graetzel, D. Sinton and E. H. Sargent, Gold-in-copper at low *CO coverage enables efficient electromethanation of CO_2, *Nat. Commun.,* 2021, **12**, 3387.

12. A. Sedighian Rasouli, X. Wang, J. Wicks, G. Lee, T. Peng, F. Li, C. McCallum, C.-T. Dinh, A. H. Ip, D. Sinton and E. H. Sargent, CO_2 Electroreduction to Methane at Production Rates Exceeding 100 mA/cm^2, *ACS Sustainable Chem. Eng.,* 2020, **8**, 14668-14673.

13. L. Xiong, X. Zhang, L. Chen, Z. Deng, S. Han, Y. Chen, J. Zhong, H. Sun, Y. Lian, B. Yang, X. Yuan, H. Yu, Y. Liu, X. Yang, J. Guo, M. H. Rümmeli, Y. Jiao and Y. Peng, Geometric Modulation of Local CO Flux in Ag@Cu_2O Nanoreactors for Steering the CO_2RR Pathway toward High-Efficacy

Methane Production, *Adv. Mater.*, 2021, **33**, 2101741.

14. S.-F. Hung, A. Xu, X. Wang, F. Li, S.-H. Hsu, Y. Li, J. Wicks, E. G. Cervantes, A. S. Rasouli, Y. C. Li, M. Luo, D.-H. Nam, N. Wang, T. Peng, Y. Yan, G. Lee and E. H. Sargent, A metal-supported single-atom catalytic site enables carbon dioxide hydrogenation, *Nat. Commun.,* 2022, **13**, 819.

15. R. M. Yadav, Z. Li, T. Zhang, O. Sahin, S. Roy, G. Gao, H. Guo, R. Vajtai, L. Wang, P. M. Ajayan and J. Wu, Amine-Functionalized Carbon Nanodot Electrocatalysts Converting Carbon Dioxide to Methane, *Adv. Mater.*, 2022, **34**, 2105690.